Kinetic Model Evaluation of the Resilience of Plasmonic Nanoantennas for Laser-Induced Fusion

István Papp,[1,2] Larissa Bravina,[4] Mária Csete,[1,5] Archana Kumari,[1,2,*] Igor N. Mishustin,[6] Dénes Molnár,[7] Anton Motornenko,[6] Péter Rácz,[1,2] Leonid M. Satarov,[6] Horst Stöcker,[6,8,9] Daniel D. Strottman,[10] András Szenes,[1,5] Dávid Vass,[1,5] Tamás S. Biró,[1,2] László P. Csernai,[1,2,3,6] and Norbert Kroó[1,2,11]
(NAPLIFE Collaboration)

[1] *Wigner Research Centre for Physics, Budapest, Hungary*
[2] *National Research, Development and Innovation Office of Hungary, Hungary*
[3] *Department of Physics and Technology, University of Bergen, Bergen, Norway*
[4] *Department of Physics, University of Oslo, Norway*
[5] *Department of Optics and Quantum Electronics, University of Szeged, Hungary*
[6] *Frankfurt Institute for Advanced Studies, Frankfurt/Main 60438, Germany*
[7] *Department of Physics, Purdue University, West Lafayette, Indiana 47907, USA*
[8] *Institut für Theoretische Physik, Goethe Universität Frankfurt, Frankfurt/Main 60438, Germany*
[9] *GSI Helmholtzzentrum für Schwerionenforschung GmbH, Darmstadt 64291, Germany*
[10] *Los Alamos National Laboratory, Los Alamos, New Mexico 87545, USA*
[11] *Hungarian Academy of Sciences, Budapest 1051, Hungary*

(Received 9 December 2021; revised 13 May 2022; accepted 20 May 2022; published 7 July 2022)

Recently, a new version of laser-induced fusion was proposed where implanted nanoantennas regulated and amplified the light absorption in the fusion target [L.P. Csernai *et al.*, Phys. Wave Phenom. 28, 187–99 (2020)]. In this paper we estimate the nanoantenna lifetime in a dynamical kinetic model and describe how electrons are leaving the nanoantenna's surface, and for how long the plasmonic effect is maintained. Our model successfully shows a nanorod antenna lifetime that will allow future fusion studies with top-energy short laser ignition pulses.

DOI: 10.1103/PRXEnergy.1.023001

I. PREVIOUS STUDIES AND RESULTS OF NANOANTENNAS AT ENERGETIC LASER IRRADIATION

Laser induced Inertial Confinement Fusion (ICF) is in a new exciting stage of development, due to the enormous increase of laser power, in particular due to the Extreme Light Infrastructure (ELI) Laboratories in the EU. Recently, NAnoPlasmonic, Laser Inertial Fusion Experiments (NAPLIFEs) were proposed [1,2] as an improved way to achieve laser-driven fusion in a nonthermal, collider configuration. While nanoantennas at intensities up to about 10^{12} W/cm^2 [3] are stable for longer irradiations, at present top intensities, these are destroyed just like the hohlraum in the experiments at the National Ignition Facility (NIF). So, the question arises if we can use nanoantennas for fusion at the top laser energies. This is only possible if the nanoantennas can survive an energetic ignition pulse that is short enough.

One of these novel ideas is the simultaneous (or "time-like") ignition [1,2], paired with enhanced energy absorption with the help of nanoantennas implanted into the target material [4]. This should prevent the development of the mechanical Rayleigh-Taylor instability. Furthermore, this also allows for a much simpler flat target configuration [5,6], utilizing a nonequilibrium, ignition dynamics. This is realized by relativistic collisions of two target slabs, produced by using the Laser Wake Field Acceleration (LWFA) mechanism [7]. The use of femtosecond laser pulses leads to rapid ignition with high, beam-directed collision velocities.

The advantages of the nonequilibrium configuration were first mentioned in Ref. [8], and experimentally tested in a linear colliding configuration [9]. The same precompression was reached as at the NIF. Recently, in the

*kumari.archana@wigner.hu

Lawrence Livermore National Laboratory the linear configuration was also tested as part of the Advanced Radiographic Capability (ARC) project [10]. In the NIF-ARC project different flat and compound parabolic concentrator target configurations were also tested [11,12], and with superponderomotive electron acceleration, proton energies > 30 MeV were reached at the relatively low laser intensity of 10^{18} W/cm^2. Several laser intensity variations in time were tested to increase the produced proton beam energies. In the NAPLIFE project [1,2], new ideas of nanoplasmonic amplification in a layered flat target with variable absorptivity to reach simultaneous ignition were applied.

The properties of resonant nanoantennas are vital for this laser-induced fusion project. In this paper the electron densities achieved in and at these nanoantennas, and their durability for energetic laser irradiation, are studied, as well as the dynamics of transient phenomena around these antennas.

The design of antennas for irradiation at optical frequencies, where the conduction band electrons in metals behave as strongly coupled plasmas [13], is the seed of this method. In-medium propagation of the laser pulse is characterized by the dielectric function $\varepsilon(\lambda)$ (its value in the infinite frequency limit is ε_∞ [14]). For gold, $\varepsilon_\infty = 11$ and the plasma wavelength $\lambda_p = 138$ nm; for silver, $\varepsilon_\infty = 3.5$ and $\lambda_p = 135$ nm [13]. The rods are embedded in a surrounding medium with dielectric constant $\varepsilon_s = \varepsilon_r\varepsilon_0$ reducing the propagation velocity of light to $c_s = 1/\sqrt{\varepsilon_s}$. This provides the refractive index $n = \sqrt{\varepsilon_s}$. Considering an antenna element as a metal rod of length L and diameter $2R$, incident light with wavelength λ moves the conduction electrons coupled with an optical electromagnetic (EM) near field (Fig. 1) to the ends, and forms a plasmonic surface charge wave. Based on these effects, the effective wavelength λ_{eff} is used in the calculations. In the case of a vacuum, $\varepsilon_r = 1$, the following three-parameter formula is given [13]:

$$\frac{\lambda_{\text{eff}}}{2R\pi} = 13.74 - 0.12[\varepsilon_\infty + 141.04] - \frac{2}{\pi} + \frac{\lambda}{\lambda_p} 0.12\sqrt{\varepsilon_\infty + 141.04}. \quad (1)$$

For golden nanorods of 25 nm diameter in vacuum, this gives an effective wavelength of $\lambda_{\text{eff}} = 266$ nm, corresponding to the length of a resonant dipole length of $L = \lambda_{\text{eff}}/2 = 133$ nm. Calculating in polymer urethane dimethacrylate (UDMA) for $n = 1.53$, L is 85 nm. As a first attempt to gain an insight into the motion of electrons in the nanoantennas, we pursue calculations with vacuum and $L = 130$ nm. The reactiveness of nanoantennas in a given medium is characterized by the fraction of the absorbed energy, the absorptivity.

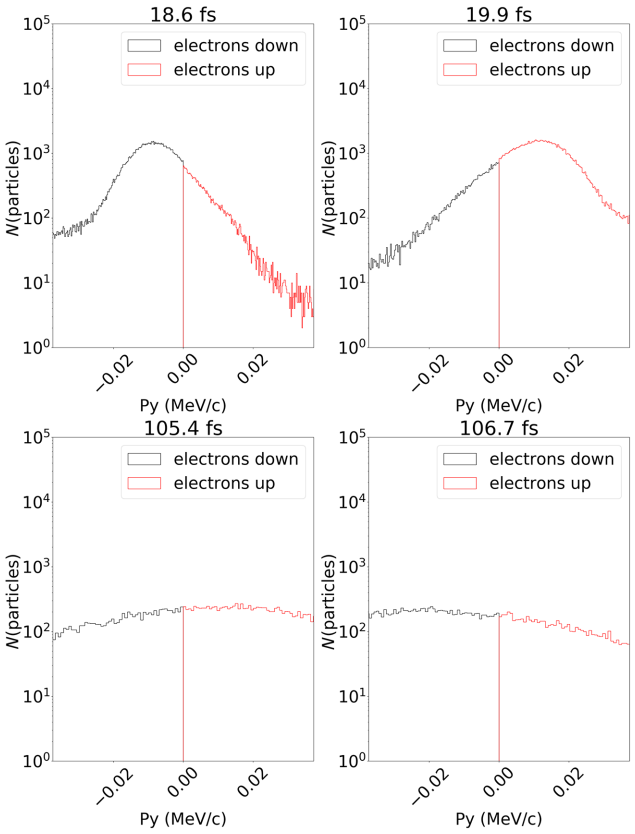

FIG. 1. A snapshot of pairs of oscillations half of a period ($T/2$) apart are shown at an earlier (top) and later (bottom) stage. The histogram of the momentum distribution is shown. Red shows the electron marker particles that are traveling up along the nanorod, while the black line shows electrons, which travel downwards. The nanorod shows the resonant oscillation; however, after around 42 fs this effect fades away with the near destruction of the nanorod. This is the lifetime of the localized surface plasmon polariton. The widening of the momentum distribution can be attributed to the kinetic model assumption, where both the conduction and binding electrons are considered freely movable. The resonance of the nanorod has a time period of $T = 2.65$ fs.

Simulation studies using COMSOL Multiphysics® with many parameters yielded absorptivities between 0.089 and 0.154 for core-shell nanoantannas and between 0.085 and 0.192 for nanorod antennas [15]. By varying the density of implanted nanoantennas one could achieve almost uniform integrated energy absorption at a given passing time of 240 fs for two counterpropagating 120 fs laser pulses.

The beam intensity should be so low that the plasmonic nanoantennas are not destroyed before the ignition pulse passes. This damage threshold depends on the geometry and size of the nanoantennas. Its knowledge is vital at low intensity but longer pulse length, picosecond or nanosecond; larger preacceleration and precompression can be reached at the price of destroying the nanoantennas.

The golden nanorods or core-shell nanoparticles may lose a few electrons from the conduction band without being destroyed in their solid structure, so they can still enhance the absorptivity of the ignition pulse for about 20–50 fs, well before the full ignition is completed in ultrashort pulse experiments. For the emission of a single electron from gold plasmonic nanoantennas, four 800 nm photons are needed. On the other hand, the incoming pulse generates a surface plasmon, which may later emit electrons. This indirect process is more frequent than the direct kick out by four photons [16,17].

Nanoantennas are very effective at absorbing the energy and momentum of light. Their absorptivity can be adjusted by regulating their implantation density in the target material. Other absorption mechanisms were considered by Balazs and Block [18–20].

II. DESCRIPTION OF THE MODEL AND METHODOLOGY

Plasmons on such nanoantennas are usually studied theoretically by solving Maxwell's equations in simulations involving finite element or finite difference time-domain methods. These approaches are efficient for computers; however, some of the important phenomena are either neglected this way or typically included by extra fitting parameters. The motion of free electrons are only taken into account indirectly via the bulk permittivity of the metal. Classical methods use the dielectric function of the free electron gas: $\epsilon(\omega) = 1 - \omega_p^2/(\omega^2 + i\gamma\omega)$ with ω_p being the plasma frequency [21], neglecting electron-electron interactions. These interactions are mimicked by using an effective mass for the electrons. Here, γ is the collision frequency, prevalent in the damping constant in the above formula. Particle simulations on the other hand use the electron number density, n_e, to randomly distribute electronlike marker particles on the metal surface.

For our simulations, we apply the particle-in-cell (PIC) method [22]. In PIC codes marker particles (representing a large number of real particles) move in continuous phase space, whereas densities and currents are computed in stationary mesh cells. We use the EPOCH multicomponent PIC code [23]. This approach proves to be efficient for analyzing the electron dynamics in different plasmon modes, and modeling electron spill-out effects [24].

In order to be close to experimental setup parameters, we choose 25 nm × 130 nm or 25 nm ∗ 130 nm not an area nanorods with resonant wavelength 800 nm. We consider three electrons in the conduction band. Irradiation is done by a 4×10^{15} W/cm^2 intensity plane wave, at 795 nm wave length and pulse duration 106 fs.

First, electrons are set inside a cylindrical rod confined with a potential-wall-like gradient of 100 V/m over 2 nm thickness on the surface, as suggested in Ref. [24], to prevent early electron escapes. Later, another approach is taken using EPOCH's built-in ion-electron collision algorithms. The method proposed by Nanbu and Yonemura takes into account Coulomb collisions based on the cumulative scattering angle [25,26].

Because of their weight, the heavy gold ions hardly move. Electrons push each other to the surface of the nanonatennas, where the attractive field of the positive gold nuclei keeps them from escaping. The electrons fluctuate between the two ends of the nanorod antennas (cf. Fig. 1), resulting in a typical electric field configuration around the nanorod antennas (see Fig. 2). At increasing laser intensities the nanorods expand slightly, and only eventually get destroyed (Fig. 1).

As seen in Fig. 2, the electromagnetic field drives the conduction electrons into resonant fluctuations. In the case of long irradiation times, $T_{\text{pulse}} \gg T$, our model describes a stationary configuration, adequate for gentle acceleration and compression. This would precede the short and extremely energetic ignition pulse in a laser wake-field collider configuration [7]. At the transition from gentle irradiation to a few femtosecond short ignition the nanoantennas must not be destroyed. The solid-state structure of the nanoantennas would be destroyed when a significant part of the electrons left the nonoantannas. This process takes a few nanoseconds, sufficient for the amplified ignition [7].

Note that, for in-medium simulations, the speed of light as well as the wave lengths are reduced by the refractive index to $c^* = c/n$ and $\lambda^* = \lambda/n$. Consequently, in a dielectric medium like UDMA the resonant antenna length is reduced by n also, and further reduced by the "thick" aspect ratio (25:75); cf. Ref. [15]. See also the introductory comments based on Ref. [13].

III. DISCUSSION AND RESULTS

By increasing the pulse intensity and duration we detect a threshold for survival of the nanonatennas; this is the main result of the present study.

Let us consider an intense laser beam ($\lambda = 795$ nm), with intensity $I = 4 \times 10^{15}$ W/cm^2, irradiating a calculation box (CB) of $S_{\text{CB}} = 530 \times 530$ nm$^2 = 2.81 \times 10^{-9}$ cm^2 cross section and of $L_{\text{CB}} = 795$ nm length, with a step-function time profile of pulse length $T_P = 106$ fs ($\approx 40\lambda/c$).

The laser energy fraction injected into this box is $E_P = 1.19$ μJ. In the geometrical middle we insert a single nanorod antenna of length 130 nm and diameter 25 nm.

As the calculation box size (λ) is 1/40th of the irradiation pulse length (40λ), the initial and final transients are of a few percent only. Without the nanorod antenna, most of the time the incoming and outgoing energy fluxes into the calculation box are the same; thus, nothing is deposited from the field energy in the box. On the other hand, when we have a nanoantenna in the middle of the box, this

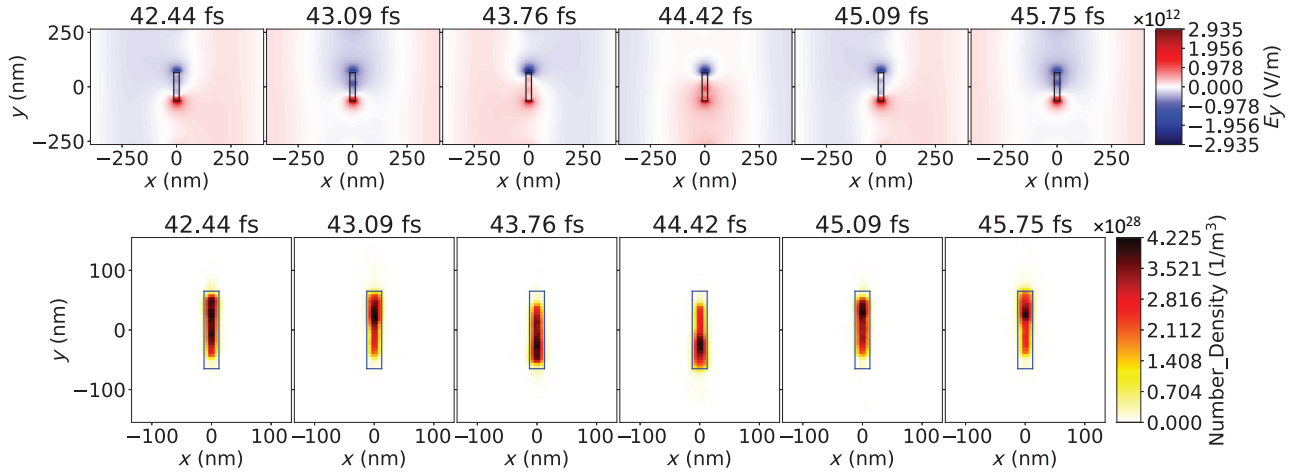

FIG. 2. Top: evolution of the E field's y component from 42.44 till 45.75 fs in a quarter of a period ($T/4 = 0.6625$ fs) steps, around a nanorod of 25 nm $\times$ 130 nm or 25 nm $*$ 130 nm indicates different parameters of the nanorod, not an area. The nanorod is orthogonal to the beam direction, x. In the transverse, $[y,z]$, plane the E field points in the y direction, while the B field points in the z direction. The external background field as well as the resonance of the nanorod reveal a time period of $T = 2.65$ fs. Bottom: the evolution of the derived number density inside the cells is shown, indicating the motion of the electron marker particles. The blue rectangle represents the boundaries of the nanorod. We note that, from 43.09 fs until 45.75 fs, a full "turn" is done by the electrons. However, at 45.75 fs the derived number density is somewhat lower (less black areas), indicating that electrons are spilled.

absorbs the energy of the EM field and converts it into plasmons and fast electrons. The amount of this absorbed energy is proportional to the energy injected at each time instant into the calculation box, leading to a monotonic decrease in the energy that remains in the field.

As shown in Fig. 3, the irradiated pulse crossing the box during $T_P = 106$ fs is $E_P = 1.19$ μJ. Thus, the average intensity of the pulse is $I_P = E_P/(S_{\rm CB}\, T_P) = 4 \times 10^{15}$ W/cm^2. The energy, since $E_{\rm CB}/E_P = 795$ nm$/(T_P\, c)$, inside the calculation box levels at $E_{\rm CB} = 30$ nJ.

Next we place a nanorod antenna of size 25 nm $\times$ 130 nm or 25 nm $*$ 130 nm orthogonal to the beam at the origo; we keep it there for the period of the irradiation, $T_P = 106$ fs. The transverse surface of the nanorod is $S_{\rm NR} = 3250$ nm^2. As we see in Fig. 3, field energy in the CB is reduced to 21 nJ, i.e., by 30%. This loss can be attributed to plasmon energy on the surface of the antenna. The transverse surface of the calculation box is given as $S_{\rm CB} = 86.4\, S_{\rm NR}$.

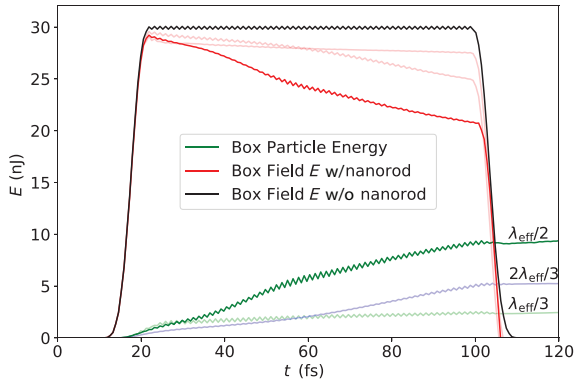

FIG. 3. The energy in the box without a nanorod antenna (black line) is constant, $E_{\rm CB} = 30$ nJ. With a nanorod antenna, part of the EM energy is absorbed (darker red line), reducing it to $E_{\rm CB} = 20$ nJ. This energy is deposited in electron motion (darker green line). Pale lines show cases of other nanorods of nonresonant lengths.

Because of a single nanorod antenna, the radiation intensity for the whole calculation box is reduced to 0.66th of the original configuration without a nanorod antenna; thus,

$$E_x = I_x\, S_{\rm NR}\, T_p = E_{\rm CB} = 0.3\, I_p\, S_{\rm CB}\, T_p. \tag{2}$$

Regarding the intensity, we estimate an enhancement of

$$I_x = 0.3\, I_p\, \frac{S_{\rm CB}}{S_{\rm NR}} = 25.9\, I_p. \tag{3}$$

Thus, the nanorod antenna in this example has a light absorption cross section, which is nearly 25.9 times larger than its geometrical cross section. This agrees with the value 21.4 received when verifying in COMSOL Multiphysics with the same nanorod. Energy is deposited as the kinetic energy of fast electrons and slow ions.

In Fig. 3 one finds that in the presence of nanoantennas the energy fluctuates with a time cycle of 2.65 fs, equal to that of the incoming laser beam. Indeed, the energy keeps the electric and magnetic fields in a linear plane wave with equal magnitudes; only their phases are shifted in a way that the intensity of radiation is constant (this is the case without nanoantennas). With nanoantennas, the much heavier gold ions also move and this modifies the

E and B fields so that their magnitudes differ permanently. Pale lines show nanorod lengths out of tune at $2\lambda_{\text{eff}}/3$ and $\lambda_{\text{eff}}/3$, i.e., 173 and 86 nm lengths, resulting in $17I_p$ and $8I_p$ intensity enhancement, respectively, i.e., less than the resonant length, $\lambda_{\text{eff}}/2$ dipole. Thus, applying optimally tuned resonant length antennas is advantageous for given nanoantenna volume or mass.

The random nanorod orientation and the beam intensity dependence have been discussed to some extent in Ref. [15].

IV. SUMMARY AND CONCLUSIONS

The model presented in this paper is certainly idealized. Our primary goal was to reproduce the behaviour of nanoantennas using a different approach from the classical one. This gives us the possibility to simulate plasmonic effects and the destruction of nanorods in a kinetic plasma environment. In reality, the nanorod antennas are implanted in random orientations, not orthogonal to the beam direction, leading to lower absorption cross sections. In our present verification experiments the amplification factor might be reduced somewhat. On the other hand, implanting more nanorod antennas would increase the total energy absorption. This amplification would increase with the density of the implanted antennas up to a saturation.

Another possibility is to have an embedding material for the target like UDMA. But such simulations are out of the scope of the traditional EPOCH code simulations where the background is a vacuum.

On the other hand, COMSOL [15] and other programs do not calculate changes in fields due to the motion of electrons and ions. The altered electron distribution, e.g., may lead to a Debye type of screening. EPOCH on the other hand evaluates such an effect. Combining these two approaches in the future may be an advantage.

The study of the dependence of laser beam intensity both theoretically and experimentally is in progress.

Another future task could arise when we have to describe the effect of preacceleration and precompression. In this case, the spherical core-shell nanoantennas become deformed and flatten, reducing the beam-directed size, while the transverse measures do not change significantly. Thus, the shape of the nanoantenna becomes a hollow torus in the transverse plane. This may even increase the gain of this antenna.

In the case of randomly oriented nanorod antennas, during compression the orientation of the antennas becomes more orthogonal to the beam. So their gain also increases. This will require further investigation.

ACKNOWLEDGMENTS

Enlightening discussions with Johann Rafelski are gratefully acknowledged. Horst Stöcker acknowledges the Judah M. Eisenberg Professor Laureatus chair at Fachbereich Physik of Goethe Universität Frankfurt. Dénes Molnár acknowledges support by the US Department of Energy, Office of Science, under Award No. DE-SC0016524. We would like to thank the Wigner GPU Laboratory at the Wigner Research Center for Physics for providing computational resource support. This work is supported in part by the Frankfurt Institute for Advanced Studies, Germany, the Eötvös Loránd Research Network of Hungary, the Research Council of Norway under Grant No. 255253, and the National Research, Development and Innovation Office of Hungary, via the Nanoplasmonic Laser Inertial Fusion Research Laboratory project (NKFIH-468-3/2021), and the projects "Optimized nanoplasmonics" (K116362) and "Ultrafast physical processes in atoms, molecules, nanostructures and biological systems" (EFOP-3.6.2-16-2017-00005).

[1] L. P. Csernai, Detonation on timelike front for relativistic systems, Zh. Eksp. Teor. Fiz. **92**, 397 (1987), and Sov. Phys. JETP **65**, 219 (1987).

[2] L. P. Csernai and D. D. Strottman, Volume ignition via time-like detonation in pellet fusion, Laser Part. Beams **33**, 279 (2015).

[3] C. Kern, M. Zürch, J. Petschulat, T. Pertsch, B. Kley, T. Käsebier, U. Hübner, and C. Spielmann, Comparison of femtosecond laser-induced damage on unstructured vs. nano-structured Au-targets, Appl. Phys. A **104**, 15 (2011).

[4] L. P. Csernai, N. Kroó, and I. Papp, Radiation-dominated implosion with nano-plasmonics, Laser Part. Beams **36**, 171 (2018).

[5] L. P. Csernai, M. Csete, I. N. Mishustin, A. Motornenko, I. Papp, L. M. Satarov, H. Stöcker, and N. Kroó, Radiation-dominated implosion with flat target, Phys. Wave Phenom. **28**, 187 (2020).

[6] A. Bonyár *et al.*, (NAPLIFE Collaboration), Nanoplasmonic Laser Fusion Target Fabrication - Considerations and Preliminary Results, Int. Conf. on New Frontiers in Physics, Kolymbari, Crete, Greece, Sept. 11, 2020.

[7] I. Papp, L. Bravina, M. Csete, I. N. Mishustin, D. Molnár, A. Motornenko, L. M. Satarov, H. Stöcker, D. D. Strottman, A. Szenes, D. Vass, T. S. Biró, László P. Csernai, and Norbert Kroó, (NAPLIFE Collaboration), Laser wake field collider, Phys. Lett. A **396**, 12724 (2021).

[8] M. Barbarino, PhD thesis, Texas AandM University, 2015.

[9] G. Zhang, *et al.*, Nuclear probes of an out-of-equilibrium plasma at the highest compression, Phys. Lett. A **383**, 2285 (2019).

[10] D. Mariscal, *et al.*, First demonstration of ARC-accelerated proton beams at the National Ignition Facility, Phys. Plasmas **26**, 043110 (2019).

[11] A. G. MacPhee, D. Alessi, H. Chen, G. Cochran, Mark R. Hermann, Daniel H. Kalantar, Andreas J. Kemp, M. Kerr, Anthony J. Link, T. Ma, Andrew J. Mackinnon, Derek A. Mariscal, D. Schlossberg, R. Tommasini, S. Vonhof, Clifford C. Widmayer, Scott C. Wilks, G. Jackson Williams,

Wade H. Williams, and K. Youngblood, Enhanced laser plasma interactions using non-imaging optical concentrator targets, Optica **7**, 129 (2020).

[12] R. A. Simpson, *et al.*, Scaling of laser-driven electron and proton acceleration as a function of laser pulse duration, energy, and intensity in the multi-picosecond regime, Phys. Plasmas **28**, 013108 (2021).

[13] L. Novotny, Effective Wavelength Scaling for Optical Antennas, Phys. Rev. Lett. **98**, 266802 (2007).

[14] M. S. Dresselhaus, Solid State Physics - Part II Optical Properties of Solids, MIT Lecture Notes, (2001).

[15] M. Csete, A. Szenes, E. Tóth, D. Vass, O. Fekete, B. Bánhelyi, I. Papp, T. Bíró, L. P. Csernai, N. Kroó, and (part of NAPLIFE Collaboration), Comparative study on the uniform energy deposition achievable via optimized plasmonic nanoresonator distributions, Plasmonics **17**, 775 (2022).

[16] M. Merschdorf, W. Pfeiffer, A. Thon, S. Voll, and G. Gerber, Photoemission from multiply excited surface plasmons in Ag nanoparticles, Appl. Phys. A **71**, 547 (2000).

[17] Gy. Farkas and Z. Gy. Horváth, Multiphoton electron emission processes induced by different kinds of ultrashort laser pulses, Opt. Commun. **12**, 392 (1974).

[18] N. L. Balazs, The energy-momentum tensor of the electromagnetic field inside matter, Phys. Rev. **91**, 408 (1953).

[19] Peter W. Milonni and Robert W. Boyd, Momentum of light in a dielectric medium, Adv. Opt. Photonics **2**, 519 (2010).

[20] Michael E. Crenshaw, Electromagnetic momentum and the energy momentum tensor in a linear medium with magnetic and dielectric properties, J. Math. Phys. **55**, 042901 (2014).

[21] S. A. Maier, *Plasmonics: Fundamentals and Applications,* (Springer Science and Business Media, New York, NY, 2007).

[22] F. H. Harlow, Hydrodynamic problems involving large fluid distortions, J. Assoc. Comput. Mach. **4**, 137 (1957).

[23] T. D. Arber, K. Bennett, C. S. Brady, A. Lawrence-Douglas, M. G. Ramsay, N. J. Sircombe, P. Gillies, R. G. Evans, H. Schmitz, A. R. Bell, and C. P. Ridgers, Contemporary particle-in-cell approach to laser-plasma modelling, Plasma Phys. Control. Fusion **57**, 113001 (2015).

[24] W. J. Ding, J. Z. J. Lim, H. T. B Do, X. Xiong, Z. Mahfoud, C. E. Png, M. Bosman, L. K. Ang, and L. Wu, Particle simulation of plasmons, Nanophotonics **9**, 3303 (2020).

[25] K. Nanbu and S. Yonemura, Weighted particles in Coulomb collision simulations based on the theory of a cumulative scattering angle, J. Comput. Phys. **145**, 639 (1998).

[26] F. Pérez, L. Gremillet, A. Decoster, M. Drouin, and E. Lefebvre, Improved modeling of relativistic collisions and collisional ionization in particle-in-cell codes, Phys. Plasmas **19**, 083104 (2012).